Supplement of Atmos. Chem. Phys., 23, 1619–1639, 2023
https://doi.org/10.5194/acp-23-1619-2023-supplement

Atmospheric Chemistry and Physics
Open Access
EGU

Supplement of

Long-term monitoring of cloud water chemistry at Whiteface Mountain: the emergence of a new chemical regime

Christopher E. Lawrence et al.

Correspondence to: Sara Lance (smlance@albany.edu)

Supplemental Figures for "Long-Term Monitoring of Cloud Water Chemistry at Whiteface Mountain: The Emergence of New Chemical Regime"

Section S1. Summary of Laboratory Methods for the Cloud Water Monitoring Program

Anions were measured using ion chromatography according to the EPA 300.1 method. Metals were measured by Inductively Coupled Argon Plasma Spectrometry or Inductively Coupled Plasma-Atomic Emission Spectrometry following the EPA 200.7 method. TOC was measured according to the EPA 450.1 method using a Tekmar Dorhmann Phoenix 800 Carbon Analyzer from 2009 to 2015. In April 2015, the system was replaced with a Teledyne Tekmar TOC Fusion Carbon Analyzer. pH and conductivity were measured according to the EPA's Aquatic Effects Research Program methodology in the Handbook of Methods for Acid Deposition Studies (US EPA Handbook, 1987). For the first two years of MADPro, pH and conductivity were measured directly in the field and at the Harding ESE Laboratory for quality assurance purposes. In 1996, the central laboratory began to only measure every 10th sample for pH and conductivity while the field measurements remained unchanged, to reduce redundancy but still retain quality assurance data. For a subset of cloud water samples collected in 2019, pH and conductivity intercomparisons were conducted between ALSC and AWI (25 cloud water samples), with slope of 1.01 ± 0.01 and $R^2 = 0.77$ for pH measurements and slope of 1.04 ± 0.023 with $R^2 = 0.93$ for conductivity measurements. Intercomparisons between ALSC and AWI for the full suite of inorganic anions, cations and TOC (10 cloud water samples) were also conducted in 2019, with SO_4^{2-} (slope = 1.13 ± 0.087, R^2 = 0.96), NH_4^+ (slope = 1.05 ± 0.030, $R^2 = 0.85$), NO_3^- (slope = 0.901 ± 0.0053, $R^2 = 0.99$) and TOC (slope = 0.998 ± 0.059, $R^2 = 0.703$).

Table S1. Summary of laboratory methods and associated method detection limits, precision and accuracy estimates used by 3 different laboratories during the cloud water monitoring program.

Mountain Acid Deposition Program (1994-2000)

Species	Method	Method Detection Limit	Precision	Accuracy
pH	pH probe	NA	5%	85-115%
Conductivity	Conductivity probe	0.2 uS cm^{-1}	5%	85-115%
SO_4^{2-}	Ion Chromatography	0.04 mg L^{-1}	5%	90-105%
NO_3^-	Ion Chromatography	0.008 mg L^{-1}	5%	95-105%
Cl^-	Ion Chromatography	0.02 mg L^{-1}	5%	95-105%
NH_4^+	Automated Phenolate	0.02 mg N L^{-1}	5%	90-110%
Ca	Inductively Coupled Argon Plasma Spectrometry	0.003 mg L^{-1}	10%	90-110%
Mg	Inductively Coupled Argon Plasma Spectrometry	0.003 mg L^{-1}	10%	90-110%
K	Inductively Coupled Argon Plasma Spectrometry	0.005 mg L^{-1}	10%	90-110%
Na	Inductively Coupled Argon Plasma Spectrometry	0.005 mg L^{-1}	10%	90-110%

Adirondack Lake Survey Corp (2001-2017, 2020-2021)

Species	Method	Method Detection Limit (mg/L)	Precision	Accuracy
pH	Orion 8102BNUWP pH probe	NA	5%	98-102%
Conductivity	YSI Model 3402 conductivity probe	0.35 uS cm^{-1}	10%	95-105%
SO_4^{2-}	Ion Chromatography	0.010 mg L^{-1}	10%	90-110%
NO_3^-	Ion Chromatography	0.024 mg L^{-1}	10%	90-110%
Cl^-	Ion Chromatography	0.012 mg L^{-1}	10%	90-110%
NH_4^+	Automated Phenolate	0.039 mg L^{-1}	10%	90-110%
Ca	Inductively Coupled Argon Plasma Spectrometry	0.012 mg L^{-1}	10%	90-110%
Mg	Inductively Coupled Argon Plasma Spectrometry	0.002 mg L^{-1}	10%	90-110%
K	Inductively Coupled Argon Plasma Spectrometry	0.005 mg L^{-1}	10%	90-110%
Na	Inductively Coupled Argon Plasma Spectrometry	0.005 mg L^{-1}	10%	90-110%
TOC (WSOC for most samples in 2020-2021)	UV/Persulfate Oxidation	0.029 mgC L^{-1}	10%	90-110%

Adirondack Watershed Institute (2018-2019)*

Species	Method	Method Detection Limit	Precision	Accuracy
pH	Mettler Toledo InLab Routine Pro electrode	NA	5%	98-102%
Conductivity	731 Mettler Toledo InLab Conductivity Probe	0.02	5%	90-110%
SO_4^{2-}	Ion Chromatography	0.09 mg/L	5%	90-110%
NO_3^-	Cadmium Reduction	0.9 µg N/L	5%	90-110%
Cl^-	Ion Chromatography	0.05 mg/L	10-15%	90-110%
NH_4^+	Semipermeable membrane+ pH indicator photometry	0.01 mg/L	5%	90-110%
Ca	Inductively Coupled Plasma-Atomic Emission Spectrometry	0.023 mg/L	5%	90-110%
Mg	Inductively Coupled Plasma-Atomic Emission Spectrometry	0.001 mg/L	5%	90-110%
K	Inductively Coupled Plasma-Atomic Emission Spectrometry	0.025 mg/L	5%	90-110%
Na	Inductively Coupled Plasma-Atomic Emission Spectrometry	0.012 mg/L	5%	90-110%
WSOC	UV/Persulfate Oxidation	0.291 C mg/L	5%	90-110%

*pH measurements in 2018 were found to suffer from a low bias compared to the measured conductivity. Archived samples were reanalyzed in the Lance Lab using separate pH (Orion 8157BNUMD ROSS Ultra pH/ATC) and conductivity (Orion 013005MD) probes, and the resulting measurements were found to be internally consistent with the other measured analytes, as shown in Figure S1. However, reanalysis could only be done on 69 of the 101 samples, due to insufficient sample volume. Thus, conductivity and pH measurements for only a subset of the 2018 samples are reported in this paper. In 2019, AWI purchased a new probe with lower detection limit, which prevented this problem from recurring.

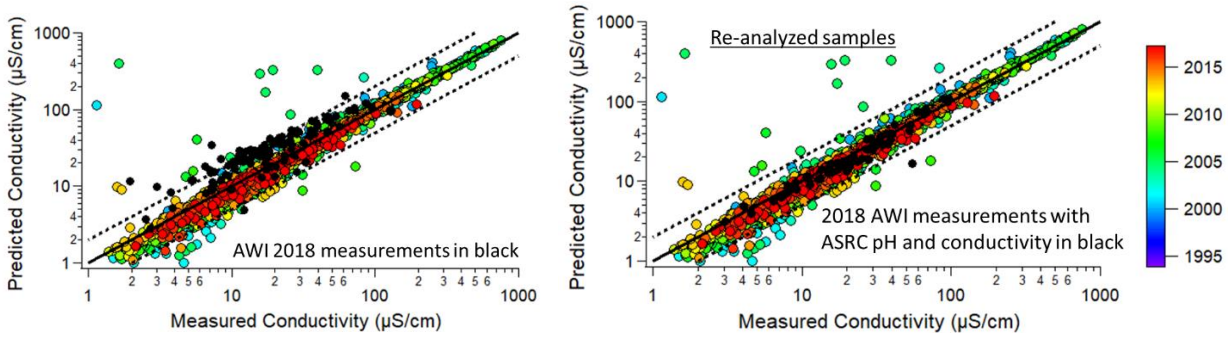

Figure S1. Predicted conductivity based on all measured inorganic cations and anions versus measured conductivity, colored by year that the cloud water sample was collected. Original AWI measurements of pH and conductivity for 2018 samples in black (left) and ASRC re-analyzed measurements of pH and conductivity for 2018 samples with sufficient remaining sample volume (right). See Section S9 for more information on the predicted conductivity calculation.

Section S2. Fraction of Measured Organic Carbon that is Water Soluble

Due the AWI filtering cloud water samples before conducting TOC analysis and the in-line cloud water filtering in 2020 and 2021, samples collected from 2018-2021 have WSOC rather than TOC reported. In order to estimate the fraction of WSOC/TOC, 38 samples collected from 2018-2019 that were analyzed for both WSOC and TOC were compared. 28 sample were measured by the Lance Lab using a Sievers 900 Portable TOC Analyzer while 10 other samples were measured by ALSC using the same methodology described in Section S1. Figures S2 plots WSOC vs TOC using an ordinary least squares regression. The slope of the regression line is 0.84 indicating the 84% of TOC is water soluble. The slope is used to estimate TOC for the trend analysis used in Figures 3 and 6.

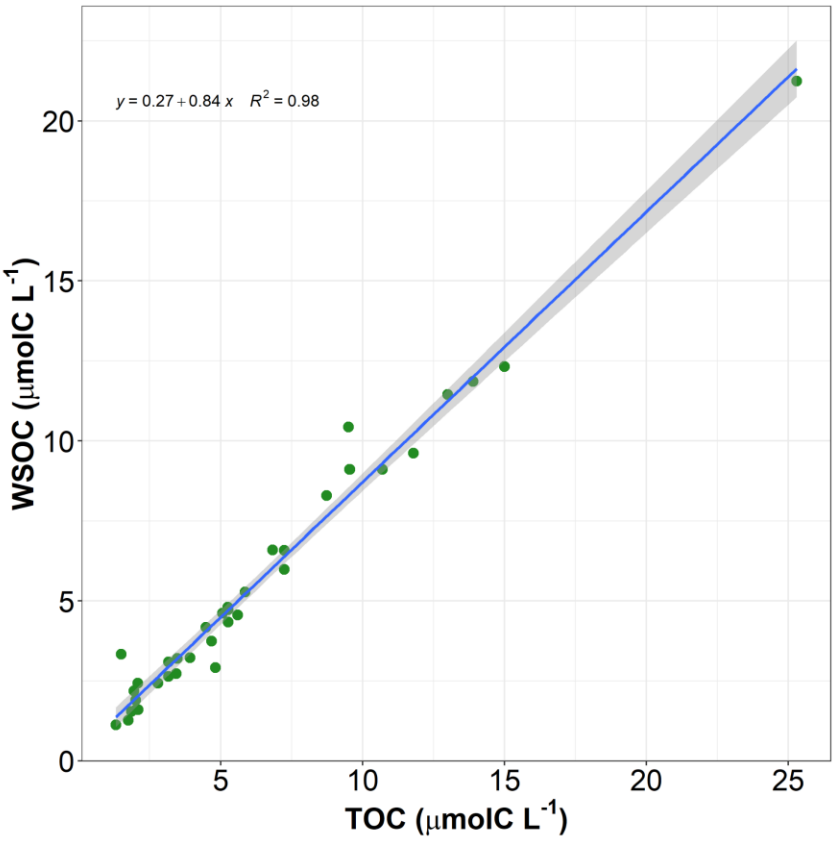

Figure S2. Measured Water Soluble Organic Carbon (WSOC) concentrations vs measured Total Organic Carbon (TOC) concentrations 38 WFM cloud samples collected in 2018 and 2019 where these measurements were obtained. WSOC is consistently 80-90% of TOC, with an average of 84%. The slope of the regression line is determined by an ordinary least squares regression.

Section S3. Seasonality of "Invalid" Samples

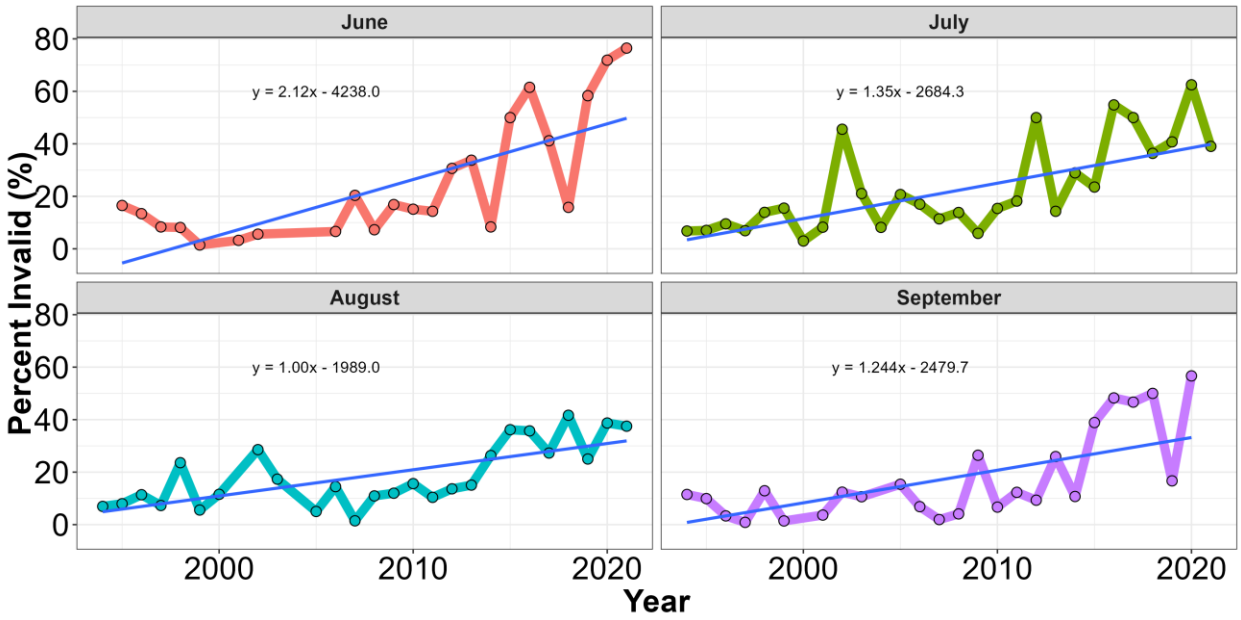

Figure S3. Percentage of cloud water samples classified as "Invalid" based on ion-balance criteria for a given month and year.

Section S4. Solubility of Ca and Mg

To assess the soluble fraction of Ca and Mg measured by Inductively Coupled Argon Plasma Spectrometry (ICAPS) and Inductively Coupled Plasma-Atomic Emission Spectrometry (ICP-AES), a Metrohm 761 Compact Cation Chromatography System was used with a Metrostep C Supp 2- 150/4 cation column to re-analyze ten unfiltered cloud samples that were archived from 2018-2020. These samples were re-analyzed twice; once unfiltered and once filtered through a 0.4 µm polycarbonate filter. The detection limits were 0.05 mg L^{-1} and 0.025 mg L^{-1} for Ca^{2+} and Mg^{2+} respectively, with a precision of 10% and an accuracy of 90-110%. The Ion Chromatography (IC) system used a 2.5 mmol L^{-1} HNO_3 eluent with 50 µg L^{-1} of $RbNO_3$. Figure S4 compares the concentrations of the unfiltered Ca^{2+} and Mg^{2+} versus the filtered Ca^{2+} and Mg^{2+}. The slope of the regression lines for both analytes are approximately 1, indicating that filtering did not have a major impact on these ion concentrations. Figure S5 shows similar regression slopes when comparing the filtered IC analysis with the original elemental Ca and Mg measurements made by ICP-AES or ICAPS, over a wide range in bulk cloud water pH. This figure provides evidence that the elemental Ca and Mg measurements were also not impacted by filtering (supporting our hypothesis that Ca and Mg are soluble in WFM cloud water).

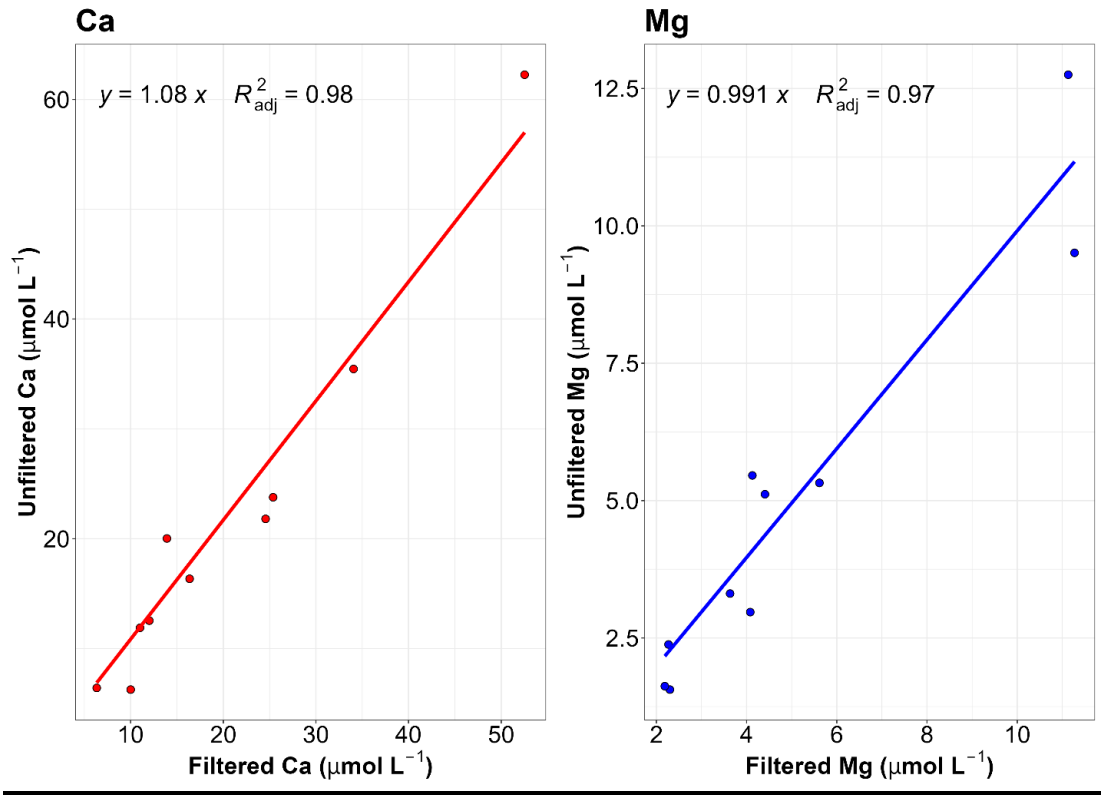

Figure S4. Comparisons of unfiltered and filtered Ca^{2+} (left) and Mg^{2+} (right) concentrations from the cation IC analysis. Agreement between these two measurements indicates that filtering did not have a major impact on the measured Mg^{2+} or Ca^{2+} ion concentrations.

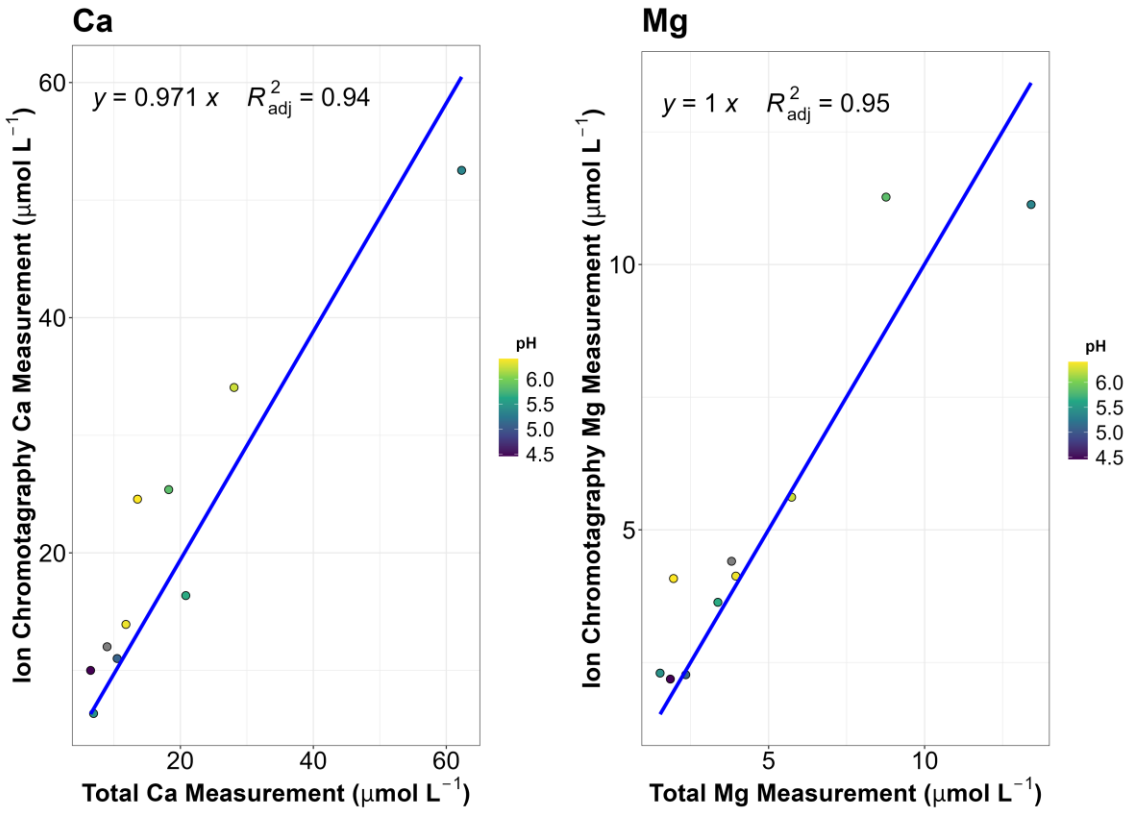

Figure S5. Comparison of filtered IC and unfiltered ICP-AES or ICAPS concentrations of Calcium (Ca, left) and Magnesium (Mg, right) concentrations, colored by the bulk cloud water pH measurements. The excellent agreement between these measurements, with pH values ranging from 4.5 to 6.4, indicates that the unfiltered Ca and Mg measurements well represent the filtered Ca^{2+} and Mg^{2+} concentrations, since all re-analyzed samples lie near to or above the 1:1 line.

The major particulate form of Ca^{2+} and Mg^{2+} are expected to be $CaCO_3$ and $MgCO_3$, which have a pH dependent solubility. The solubility of $CaCO_3$ or $MgCO_3$ can be calculated by:

$$[X] = \frac{[CO_3^{2-}]}{Ksp}$$

[X] is the molar concentration of Ca^{2+} or Mg^{2+} and Ksp is the solubility product of $CaCO_3$ (K_{sp} = 4.67×10^{-9}) or $MgCO_3$ (K_{sp} = 6.82×10^{-6}). $[CO_3^{2-}]$ can be estimated using the partial pressure of atmospheric CO_2 and the equations from the carbonate equilibrium:

$$[H_2CO_3] = \frac{K_H}{P_{CO2}}$$

$$Ka_1 = \frac{[H^+][HCO_3^-]}{[H_2CO_3]}$$

$$Ka_2 = \frac{[H^+][CO_3^{2-}]}{[HCO_3^-]}$$

Where K_H ($3.4x10^{-2}$) is the Henry's law constant of CO_2, and P_{CO2} is the partial pressure of CO_2 (assumed to be 410 ppm), Ka_1 is the acid dissociation constant of H_2CO_3 ($4.37x10^{-7}$), and Ka_2 ($5.01x10^{-11}$) is the acid dissociation of HCO_3^-. All constants are assumed to be at 25 ºC
The total amount of $CaCO_3$ and $MgCO_3$ that dissolves at equilibrium with the atmosphere as function of pH can then be calculated as

$$[X] = \frac{K_{sp}[H^+]^2}{Ka_1 Ka_2 K_H P_{CO2}}$$

Figure S6 shows the solubility of Ca and Mg vs pH. These calculations indicate that even at the highest measured concentrations of Ca and Mg and the highest measured pH values (which do not occur on the same date), $CaCO_3$ and $MgCO_3$ are expected to be fully dissolved. Other known alkaline Earth metal salts, like $CaNO_3$, $CaCl_2$ or $CaSO_4$ are even more soluble than $CaCO_3$.

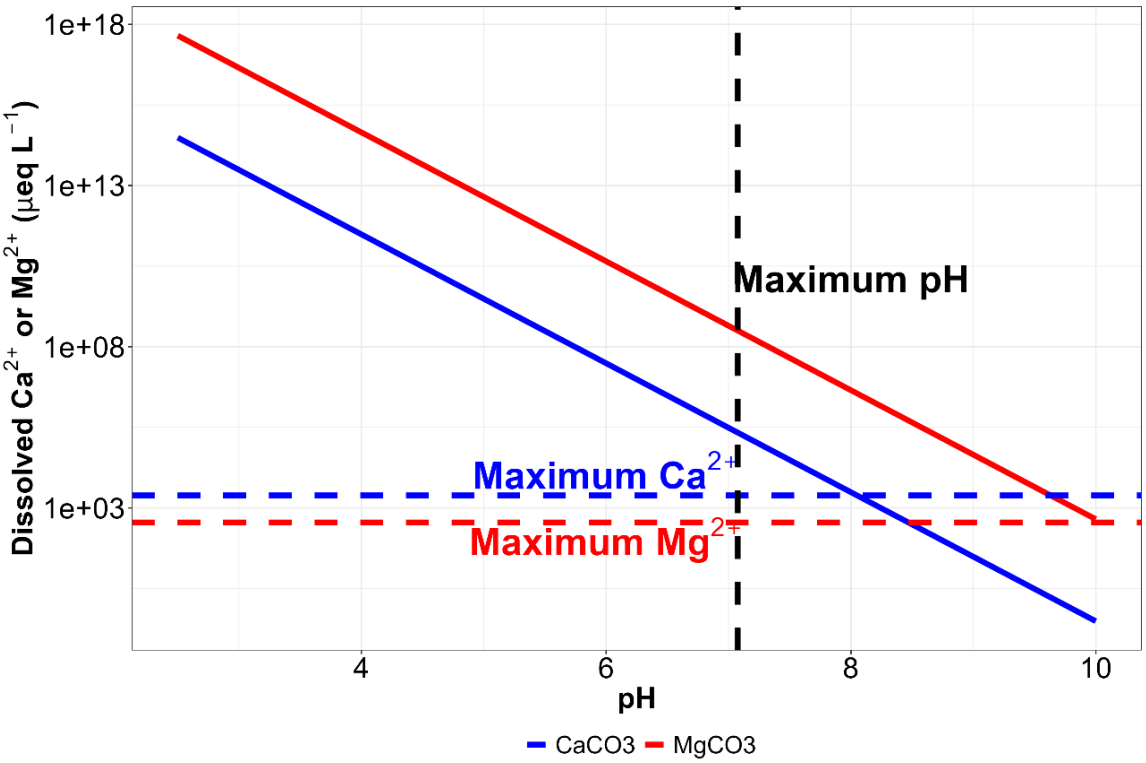

Figure S6. Solubility of $CaCO_3$ and $MgCO_3$ as a function of pH. The solid red and blue lines represent the total amount of Ca^{2+} and Mg^{2+} that can be dissolved at a given pH while the dashed blue and red lines represent the maximum concentrations of Ca^{2+} and Mg^{2+} measured in WFM cloud water and the dashed black line represents the highest ever measured pH value.

Based on both the comparisons of filtered IC measurements of Ca^{2+} and Mg^{2+} concentrations with unfiltered ICP-AES and ICAPS measurements of total Ca and Mg (over a very wide range in pH) and the equilibrium calculations shown above, we assume that the historical measurements of Ca and Mg concentrations are in their ionic forms and can be included in the overall ion balance calculations, as has been done by other researchers for many years.

Section S5. Calculating an average cloud LWC for each cloud water sample

An average LWC was recorded in the long-term cloud water dataset for each bulk cloud water sample. However, the details behind how this value was determined were not recorded. There is some indication that these average LWC values were calculated by including all LWC values ≥ 0.05 g m^{-3}. However, This calculation may lead to a high bias by including rain events, during which the collector was not actually deployed. To ensure that LWC values measured during rain events aren't included in the LWC averaging, we recalculate the average LWC from 2009 to 2021 based on the available hourly meteorology data. The cloud water data prior to 2009 does not include when the collector was deployed, making measurements prior to 2009 subject to greater uncertainty. In our recalculation, hourly LWC values were only included in the 3 or 12 hour average if: 1) LWC ≥ 0.05 g m^{-3}, 2) the cloud water collector was deployed > 25% of the time and 3) rain was detected < 15% of the time.

The performance of this algorithm was tested using 1-minute resolution data available for the 2016 collection season. Figure S7 compares the recalculated average LWC values to the average LWC determined from the 1-minute resolution LWC data for every minute the cloud collector was deployed. This demonstrates that accounting for deployment time and rain detection reduces bias and random error of the LWC values. Recalculated average LWC values that follow the criteria above are colored red, while blue data points represent the cloud water samples that would be excluded from the CWL. Using this methodology, approximately 29% of cloud water samples are removed from analysis due to the inclusion LWC values while the collector was not deployed.

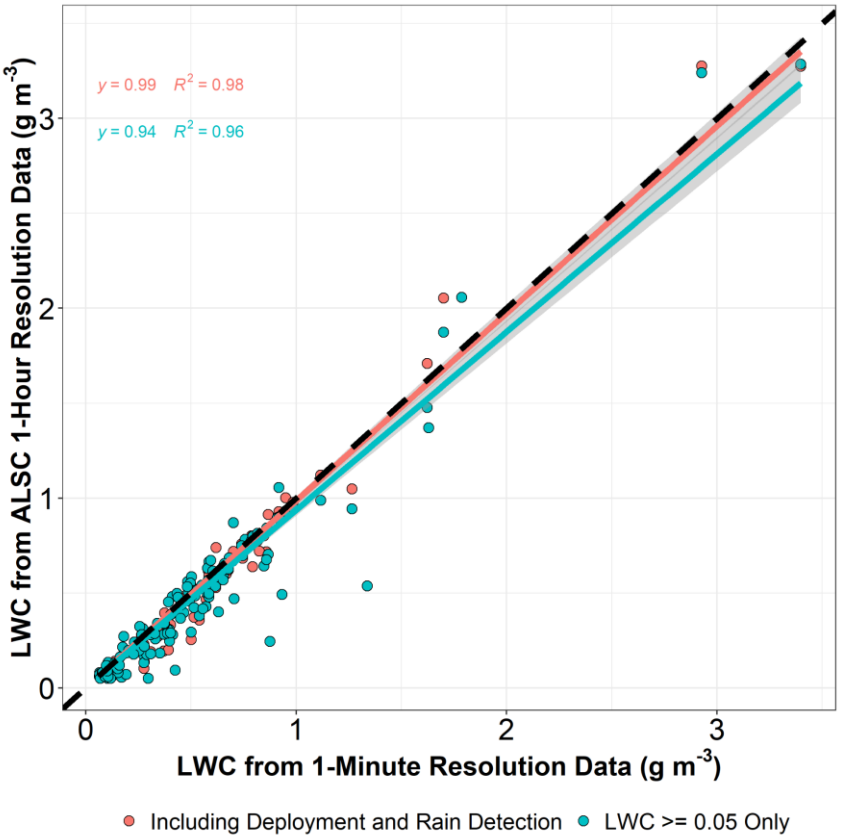

Figure S7. 12 hourly averaged LWC recalculated based on the hourly LWC data reported by ALSC in 2016 vs 12 hourly averaged LWC calculated based on 1-minute LWC measurements only when the cloud water collector was deployed. Blue points represent LWC averages when LWC > 0.05 g m^{-3} while the red points represent LWC averages when all conditions of:LWC > 0.05 g m^{-3}, the cloud collector is deployed for > 25% of the time, and rain is detected < 15% of the time are met. When accounting for time when the cloud water collector isn't deployed in addition to LWC improves the relationship between the ALSC reported LWC and minute resolution LWC. In addition, LWC values with values above 2 g m^{-3} were not included in the LWC_{samp} calculation based on the reasonable assumption of rain.

Section S6. Comparing "Valid" versus "Invalid" data sets

Another consideration for assessing measurement validity based on ion balance criteria alone is that complete chemical analysis requires a minimum volume of water (100-250mL). If a given analyte could not be measured due to inadequate sample volume, the sample would be considered "Invalid" by default simply because ion balance could not be assessed. This protocol resulted in observational bias for samples where sufficient cloud water was collected for full analysis, which typically correspond to clouds with higher liquid water content (LWC) and/or longer collection intervals.

Table S2: Theil-Sen regression slopes and associated Mann-Kendall test p-values for the a) valid and b) complete cloud water datatsets.

a) Theil-Sen Slope and Mann Kendall P-Value Valid Dataset

Analyte	*Slope*	*P-Value*
pH (units/yr)	0.0514	p < 0.001
Conductivity (uS/cm yr)	-2.2863	p < 0.001
SO4 (ueq/L yr)	-5.1386	p < 0.001
NO3 (ueq/L yr)	-1.7642	p < 0.001
NH4 (ueq/L)	-2.0083	p < 0.001
TOC (umolC/L yr)	9.2176	p < 0.001
Ca (ueq/L yr)	0.1389	0.199
Mg (ueq/L yr)	0.0272	0.172
K (ueq/L yr)	-0.0009	0.906
Na (ueq/L yr)	-0.0187	0.259
Cl (ueq/L yr)	-0.0956	0.00267

b) Theil-Sen Slope and Mann Kendall P-Value Complete Dataset

Analyte	*Slope*	*P-Value*
pH (units/yr)	0.0547	p < 0.001
Conductivity (uS/cm yr)	-1.9741	p < 0.001
SO4 (ueq/L yr)	-4.1326	p < 0.001
NO3 (ueq/L yr)	-1.3485	p < 0.001
NH4 (ueq/L)	-1.2964	0.00603
TOC (umolC/L yr)	22.4134	p < 0.001
Ca (ueq/L yr)	0.4947	p < 0.001
Mg (ueq/L yr)	0.1174	0.00126
K (ueq/L yr)	0.0198	0.0819
Na (ueq/L yr)	0.0050	0.782
Cl (ueq/L yr)	-0.0553	0.0313

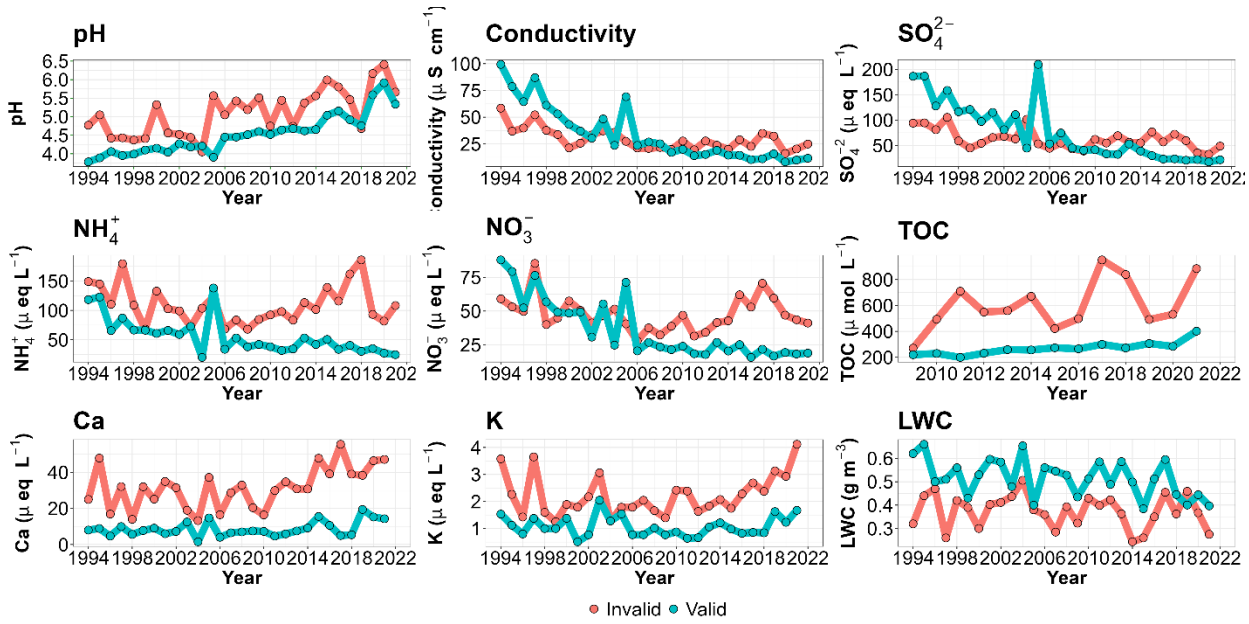

Figure S8. Comparisons between the so-called "Valid" and "Invalid" data sets for annual median concentrations of six analytes of interest, conductivity, pH and LWC.

Some analytical laboratories handle data quality control differently, for example by repeating measurements when ion balance for a sample is not attained, and nevertheless classifying the data for that sample as valid if the subsequent measurements match the initial measurements. Unfortunately, retesting the old cloud water samples collected at WFM is not possible, as the samples have not been archived, and repeat testing would again skew the statistics toward samples with greater volume of collected cloud water (since repeat testing would not have been possible for the lowest volume samples).

Across all years, annual median LWC is higher within the "Valid" data set. Higher LWC tends to correspond to more dilute samples, thereby reducing concentrations (Aleksic et al., 2010). Changes in LWC, however, do not explain the divergence in analyte concentrations starting around 2006 between the "Valid" and "Invalid" data sets since the LWC trends do not diverge and instead remain relatively unchanged.

Section S7. Seasonality of TOC Trends

Figure S9 shows the annual median trends of TOC concentrations, split up by month. Theil-sen regression analysis reveals that June, July, and September have a statistically significant increasing trend of TOC (p = 0.00493, 0.00414, and 0.012 for June, July, and September). June and July typically exhibit higher concentrations of TOC than August and September and are the main drivers of the increasing TOC trend.

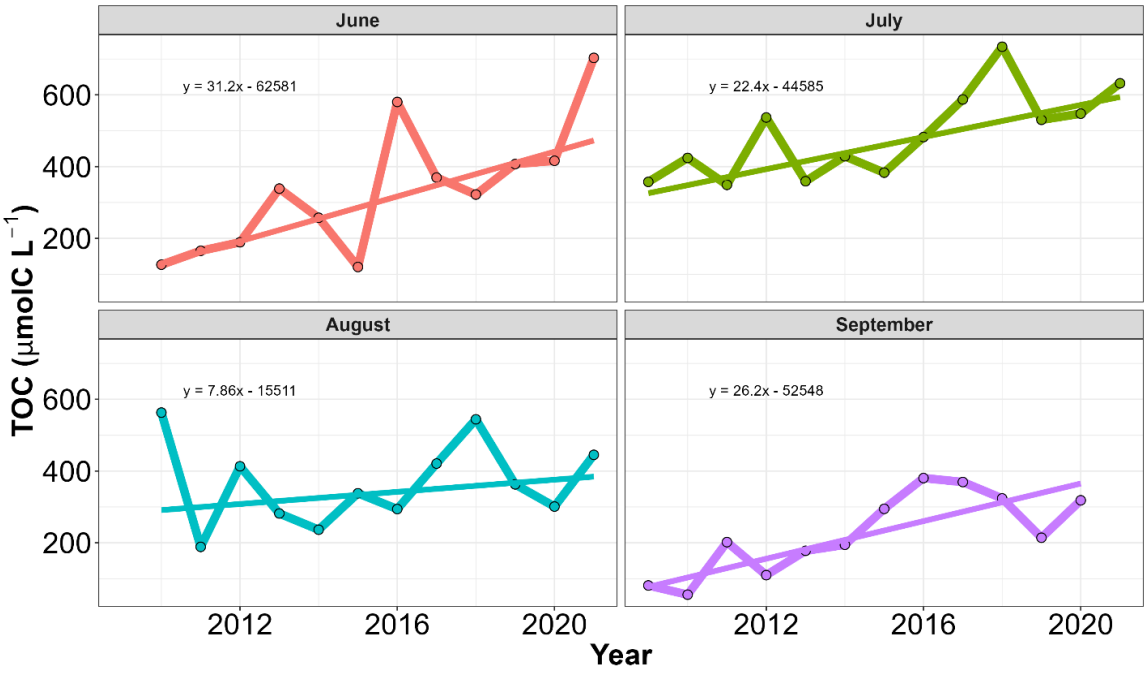

Figure S9. Annual median TOC concentrations by month.

Section S8. Impact of LWC on total ion content and total organic carbon concentrations

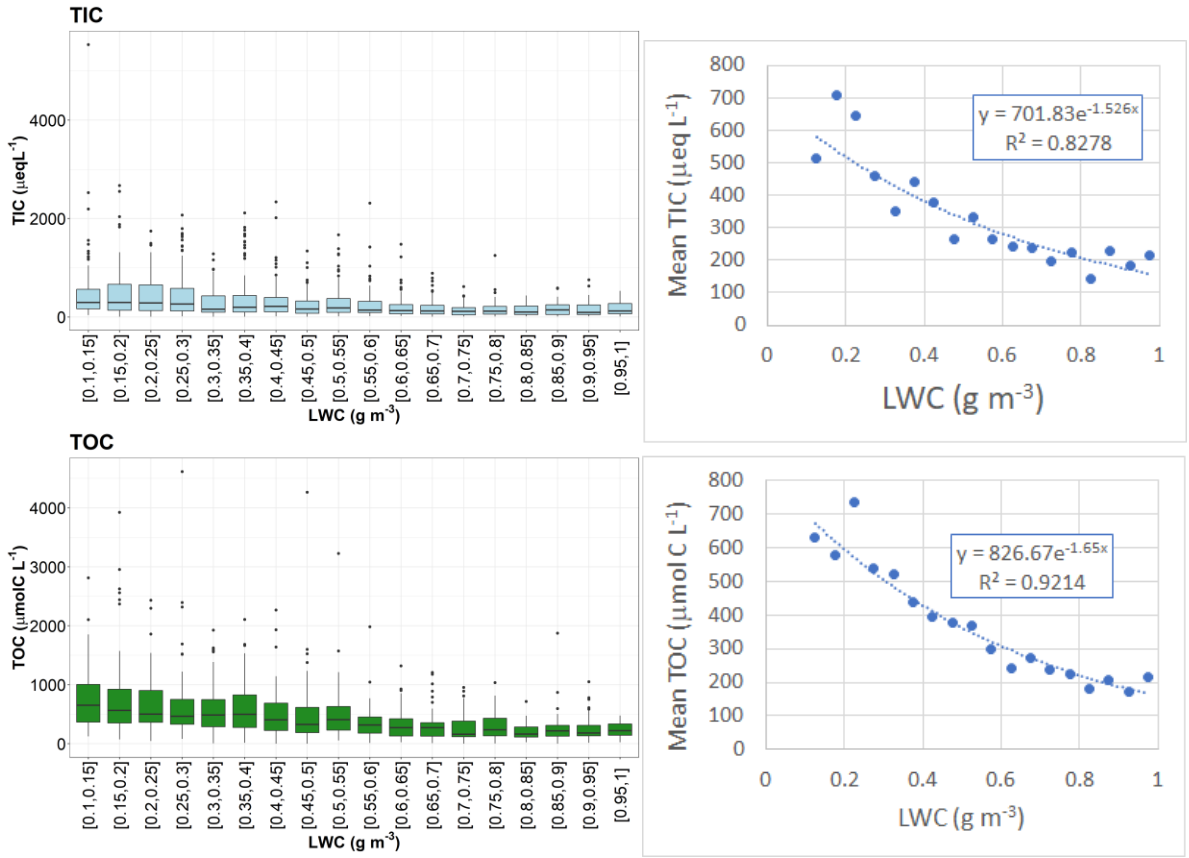

Figure S10. Total Ion Concentration (TIC) and TOC concentrations vs LWC using a similar binning procedure as described in Aleksic and Dukett (2010). With the exception of the lowest LWC bins, there is a general decrease in TIC and TOC concentrations as LWC increases. Within each LWC bin, there is considerable variability.

Table S3. Theil-Sen regression slope and associated Mann-Kendall p-values for cloud water loadings for the years 2009-2021.

Theil-Sen Slope and Mann Kendall P-Value Cloud Water Loadings

Analyte	*Slope*	*P-Value*
LWC (g/m^3 yr)	-0.00240	0.36000
SO4 (ug/m^3 yr)	-0.02960	0.02400
NO3 (ug/m^3 yr)	0.01560	0.24600
NH4 (ug/m^3 yr)	0.00112	0.66900
TOC (ug/m^3 yr)	0.07300	0.09950
Ca (ug/m^3 yr)	0.01490	0.00186
Mg (ug/m^3 yr)	0.00202	0.01730
K (ug/m^3 yr)	0.00151	0.00414
Na (ug/m^3 yr)	0.00158	0.00186
Cl (ug/m^3 yr)	0.00128	0.05860

Section S9. Two independent measures that suggest missing analytes are pH dependent

The ratio of measured cations to measured anions tends to increase with measured pH for all years of the study (Figure S11), and nearly all samples exhibit more measured cations than anions for pH ≥ 5.5. As noted in the manuscript, greater measured cations than anions suggests that there are anions present in solution that are not being measured with the current suite of instruments. Within the past decade, the Cation/Anion ratio was almost always > 1, even at pH as low as 3.5. Many of the older samples also exhibited Cation/Anion ratios as high as 3 at pH of 5. The cation and anion concentrations versus pH are further explored in Figure S12 and S14.

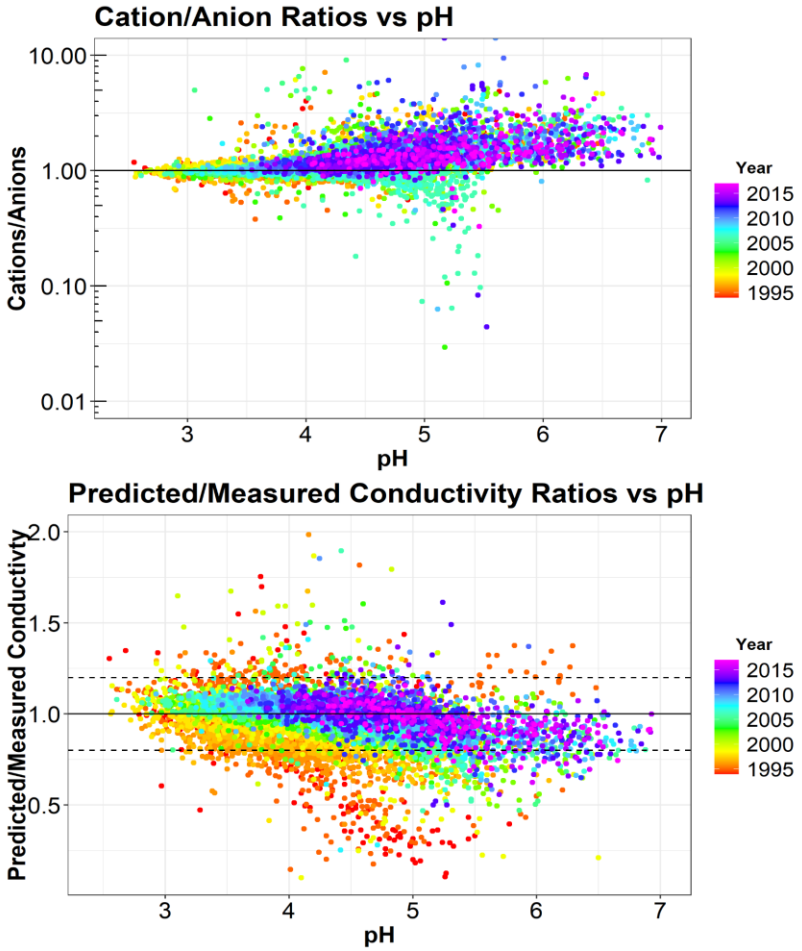

Figure S11. Cation/Anion ratio versus pH (top) and Predicted/Measured Conductivity vs pH (bottom) colored by the year the sample was collected, for all cloud water samples from 1994-2017. The dotted lines show 20% uncertainty in Predicted/Measured conductivity.

Also shown in Figure S11 is the ratio of predicted conductivity to measured conductivity versus pH. Predicted conductivity is calculated using the concentrations of measured cations and anions and their associated limiting molar conductivities. The first few years of data shows greater variability both above and below predicted/measured conductivity of 1, suggesting that the

conductivity measurement uncertainties were higher in the earliest years of the cloud water collection program. Note that since at least 2006, nearly all samples with pH > 5.5 exhibited higher measured conductivity than predicted from the measured analytes. Systematic underprediction of the measured conductivity suggests the presence of ions that are not being measured. On the contrary, samples with pH < 4 tended to exhibit lower conductivity than predicted from the measured analytes, especially in recent years. Overprediction of conductivity might be due to the presence of organic molecules like sugars and starches that can lower the conductivity of a salt solution (Kaewthong and Wattanachant, 2018). This potential effect could be dampening the impact of missing analytes on the underprediction of conductivity at high pH.

Section S10. Potential impact of bicarbonate ion concentrations on ion imbalance

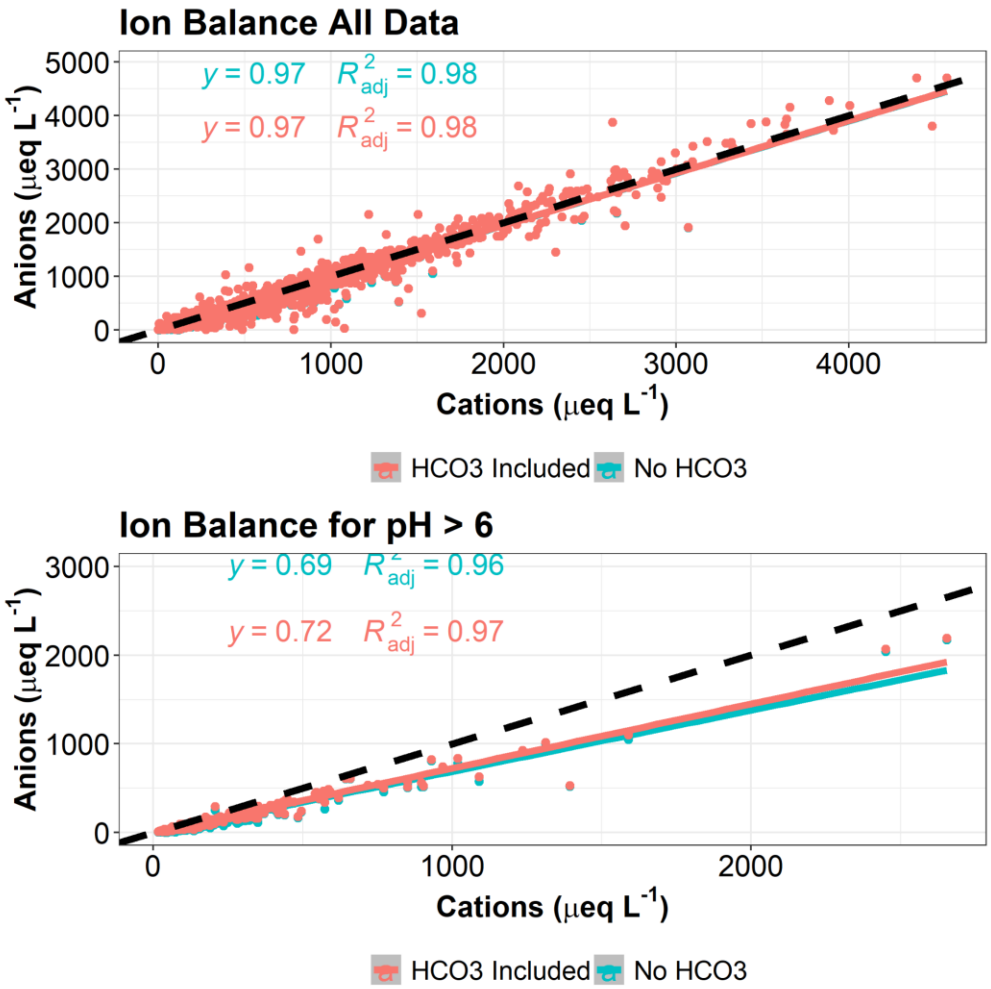

Figure S12. Anions vs Cations when including HCO_3^- within the ion balance for the entire dataset (top) and for samples that have measured bulk cloud water pH values > 6 (bottom). There are virtually no changes in ion balance for the vast majority of samples, but for pH values > 6 there is a slight impact.

Section S11. Ion Imbalance relationship with TOC

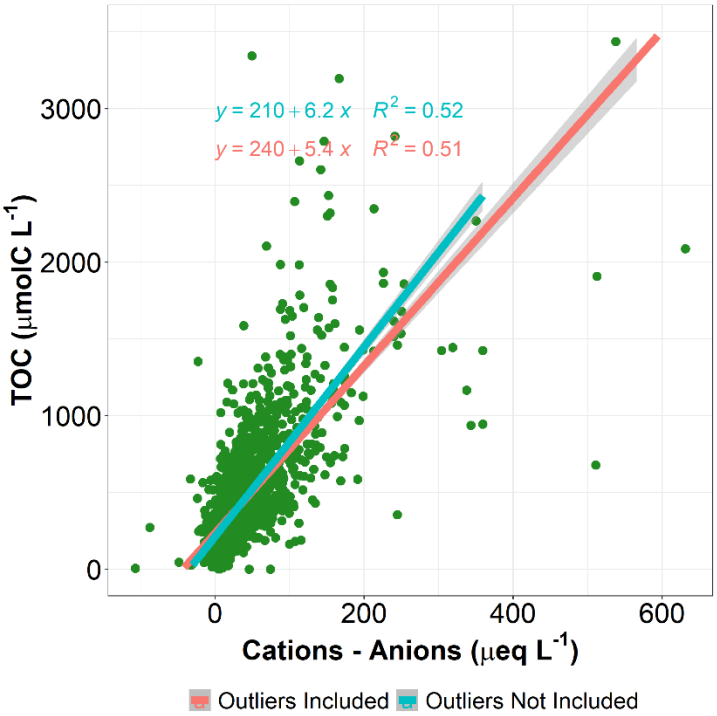

Figure S13. Measured TOC concentrations versus Ion Imbalance, i.e. measured Cations - Anions, for all cloud water samples from 2009 to 2021. Regression lines are calculated using ordinary least squares regression. A strong positive relationship between TOC and ion imbalance suggests that unmeasured organic compounds are a significant contributor to ion balance. There are 4 potential outliers with > 400μeq/L ion imbalance that could lead to a low bias in the slope of the regression. To account for this, regression lines were calculated including and excluding these potential outliers. The inclusion of the outliers led to a slightly decreased slope, and had virtually no change in the R^2 value, indicating that the outliers had little impact on the regression line.

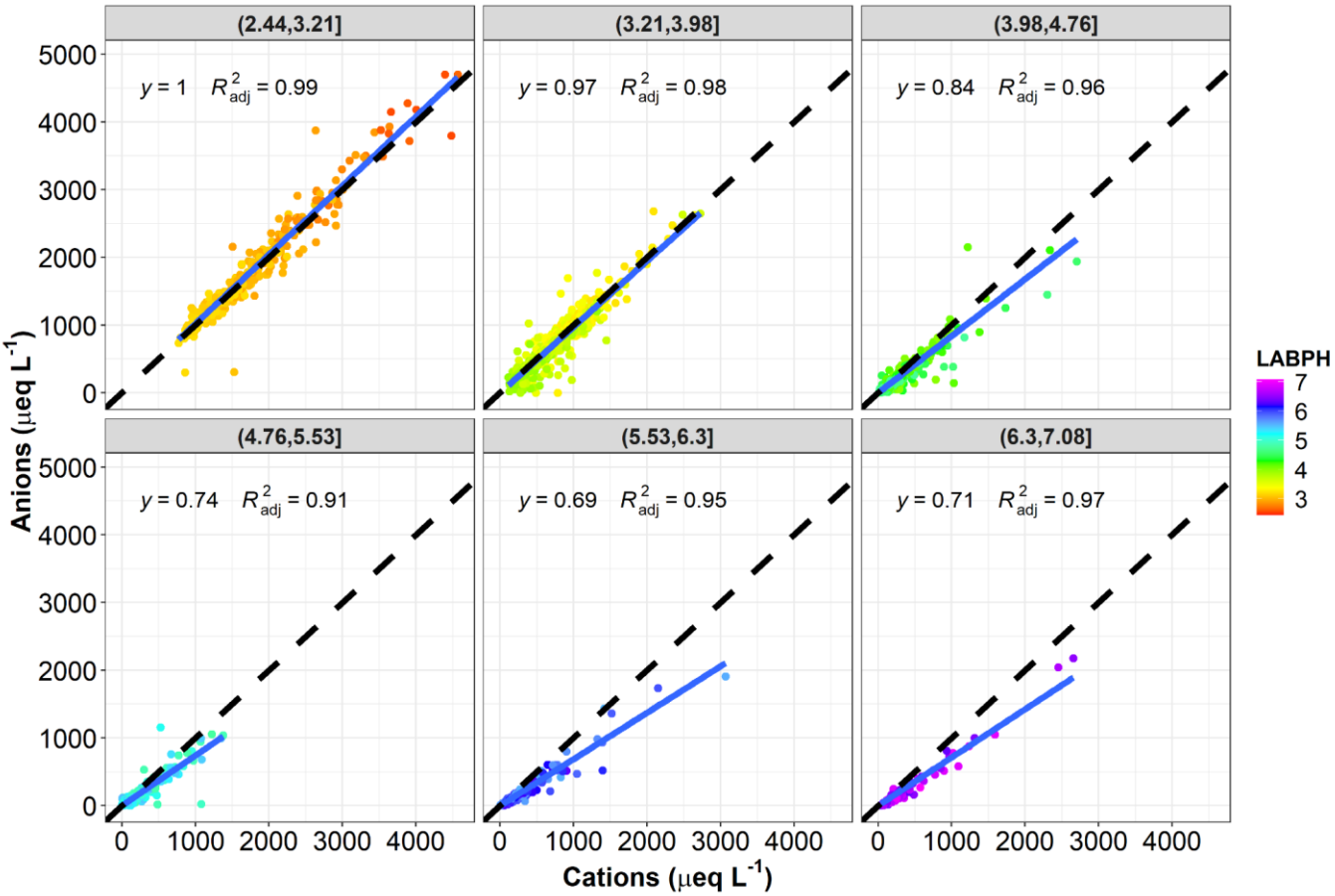

Figure S14. Anions vs Cations, split into 6 pH bins for Valid and Invalid cloud water samples collected from 1994-2021. As pH increases, there is a clear drop in the slope of the line. The largest decreases in slope occur in the bin of 3.98-4.76 and 4.76-5.53, which coincides with the pKas of formic and acetic acid (3.74 and 4.75 respectively), the two most common organic acids for in cloud water samples. As the pH increases, the fraction of these acids that are in their anionic forms increases. The increasing ion imbalance as pH increases could be evidence of greater fraction of organic acids existing in their ionic form, thus contributing to a growing ion imbalance.

Section S12. Abundance of organic acids required to reconcile observed ion imbalance, versus likely abundance of organic acids given observed OC

Figure S15 shows a potentially growing fraction of TOC that is ionic (p = 0.0327), based on the inorganic ion imbalance divided by the measured TOC concentrations, applying various assumptions for the carbon to charge (C/z) ratio of dissolved organic molecules (ranging from one to five carbon atoms on average per organic acid functional group). The calculated contribution of organic ions to TOC peaks in 2020 where 12%-58.0% of TOC is estimated to be ionic. These results suggest that not only is TOC increasing in cloud water at WFM but an increasing fraction of TOC may be ionic.

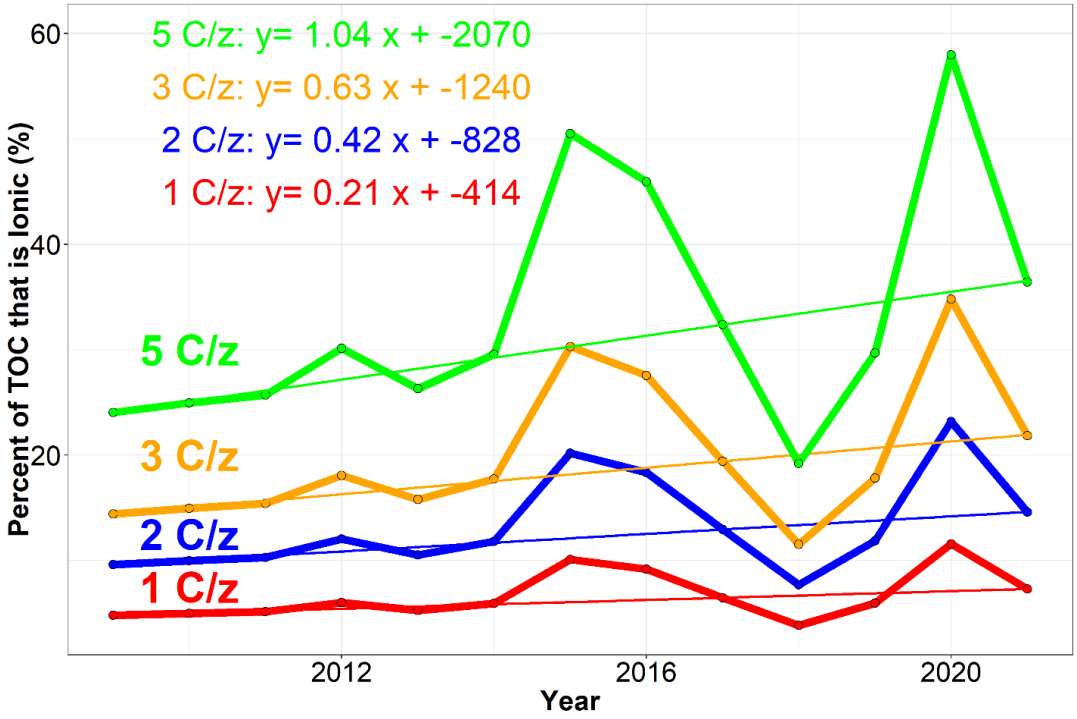

Figure S15. The annual median percent of TOC that is ionic as a function of the carbon to charge ratio (C/z)

Section S13. Size-resolved Aerosol Composition

Aerosol composition as a function of dry particle size is needed to better interpret the cloud water dataset. Since this information is not currently available from the summit of WFM, nor was this information available when the long-term cloud water data set was obtained, we looked for size resolved aerosol composition measurements conducted within the region. Measurements conducted mostly in Toronto, Ontario were referenced several times in the paper, as they show both the base cation mass distributions and organic acid mass distributions with respect to the dry aerosol (VandenBoer et al., 2011). These measurements were obtained during the measurement period of the current study. This dataset was re-evaluated for our specific purposes. As noted in the manuscript, 65-95\% of the total aerosol Ca^{2+} mass and 78-99 of Mg^{2+} were within super micron (> 1 um) aerosol in 2009-2010 when those measurements were conducted (VandenBoer et al., 2011). However, > 99% of the total number of aerosol were found in sub-micron particles.

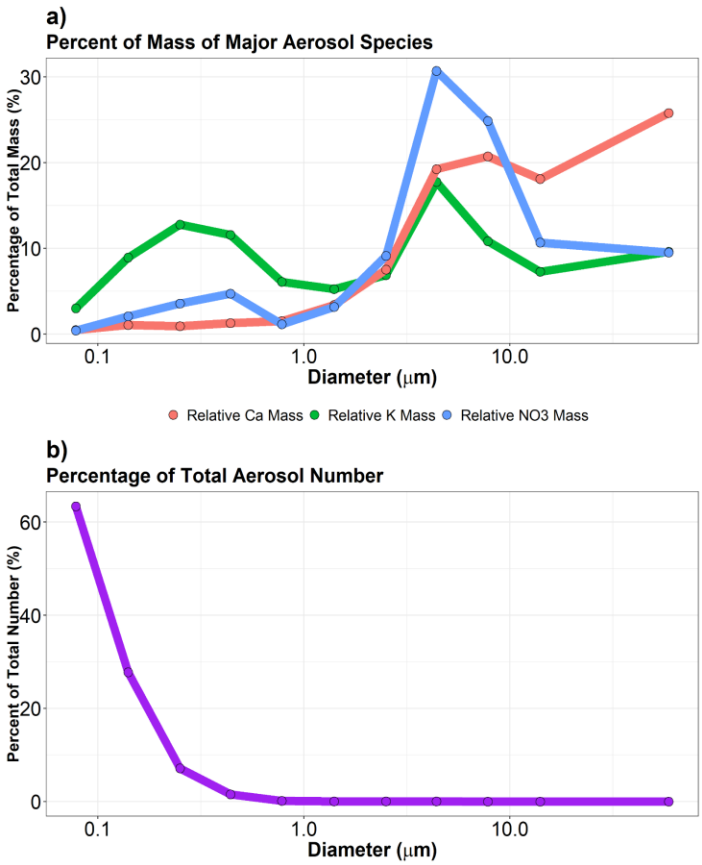

Figure S16. a) Normalized mass distributions of Ca^{2+} (red), NO_3^- (blue) and K^+ (green) as a function of particle diameter based on measurements in Toronto, Dorset, Lambton Shores, and Egbert in 2009 (VandenBoer et al., 2011). These observations show that the vast majority of Ca^{2+} mass is contained in aerosol with diameters > 1 μm, while K^+ exhibits a bimodal distribution, with significant proportions of

mass contained in diameters above and below 1 μm. NO_3^- is also largely contained in aerosol with diameters > 1 μm in the plot above, but with substantial variability sample to sample. b) Calculated percent of total aerosol number as a function of particle diameter, based on the total measured aerosol mass and an estimate for the particle density.

A wide range (11-71%) of K^+ was found to reside in super micron aerosol, suggesting that while a significant fraction of K^+ can be associated with mineral dust, an important fraction can also come from non-dust sources like biomass burning. The fraction of NO_3^- within coarse mode aerosol was also found to be highly variable, ranging from 21-93\%. While NO_3^- often resides within fine mode aerosol, gaseous HNO_3 can react with coarse mode aerosol containing alkaline species like $CaCO_3$ and $MgCO_3$ (Hansen et al., 2010, Hrdina et al., 2021) resulting in a significant amount of coarse mode aerosol NO_3^- (Fig. S16).

Section S14. Impact of pH proxies in Linear vs. Nonlinear Regimes

The large and growing discrepancy between bulk cloud water pH, pH_{TD} and pH_{BU} over the past decade coincides with a growing fraction of samples being characterized in the Non-Linear Regime. We propose that, with SO_4^2 concentrations decreasing at the same time TOC and base cation concentrations have been increasing, the major influences on cloud droplet pH are also changing. When we segregate individual cloud water samples by the Linear and Non-Linear regimes (Fig. S17, left and right, respectively), we can more clearly see how the different pH proxies compare. Within the Linear Regime, $[H^+]_{BU}$ (plotted on the x-axis) shows a strong correlation with measured bulk cloud water $[H^+]$, with slight (11%) overprediction from SO_4^{2-}, NO_3^- and NH_4^+ concentrations. Removing the influence of coarse mode aerosols by including Ca^{2+} and Mg^{2+} in the $[H^+]_{TD}$ calculation improves the agreement to a nearly 1:1 relationship between $[H^{+\$}]_{TD}$ and $[H^+]_{BU}$. Within the Non-Linear Regime, $[H^+]_{BU}$ greatly overpredicts measured bulk cloud water acidity. When removing the influence of course mode aerosol, the correlation improves substantially, with slight underprediction (14%) from SO_4^{2-}, NO_3^- and NH_4^+ concentrations. As noted previously, $[H^+]_{BU}$ can only include samples where $[SO_4^{2-}]+[NO_3^-] > [NH_4^+]$, which removes a growing fraction of samples from the analysis, potentially underestimating the fraction of acidity from unmeasured ions in the system. A Theil-Sen Regression was used to provide a robust estimate of the slope between $[H^+]_{BU}$ and measured bulk cloud water $[H^+]$ and $[H^+]_{TD}$. This method was used to reduce the impact from outlier samples on the regression line, particularly within the Non-Linear regime.

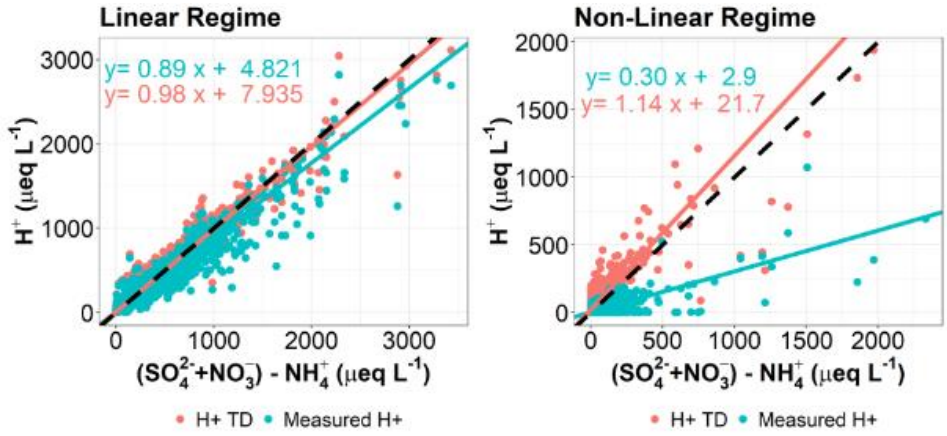

Figure S17. Measured $[H^+]$ and estimated cloud droplet $[H^+]$ versus $[SO_4^{2-}]+[NO_3^-]-[NH_4^+]$ for the Linear and Non-Linear regimes (left and right, respectively). Slopes of the regression lines are calculated using a Theil-Sen regression. The dashed line represents a 1:1 line, when $[SO_4^{2-}]+[NO_3^-]-[NH_4^+]$ perfectly predicts H^+. Only samples where $[SO_4^{2-}]+[NO_3^-]-[NH_4^+] > 0$ are used in the regression.

In the Linear Regime, $SO_4^{2-} + NO_3^- - NH_4^+$ is a useful predictor for both measured bulk cloud water pH and estimated cloud droplet pH. In the Non-Linear Regime, the relationship with measured pH is very weak. The relationship improves when using inferred cloud droplet pH, but underpredicts measured cloud droplet pH. This analysis reveals a missing source of acidity that correlates with TOC, which needs to be accounted for as a majority of cloud water samples are now within the Non-Linear Regime.

Section S15. Measured and Estimated Cloud Droplet pH versus LWC, NH_4^+ and NO_3^-

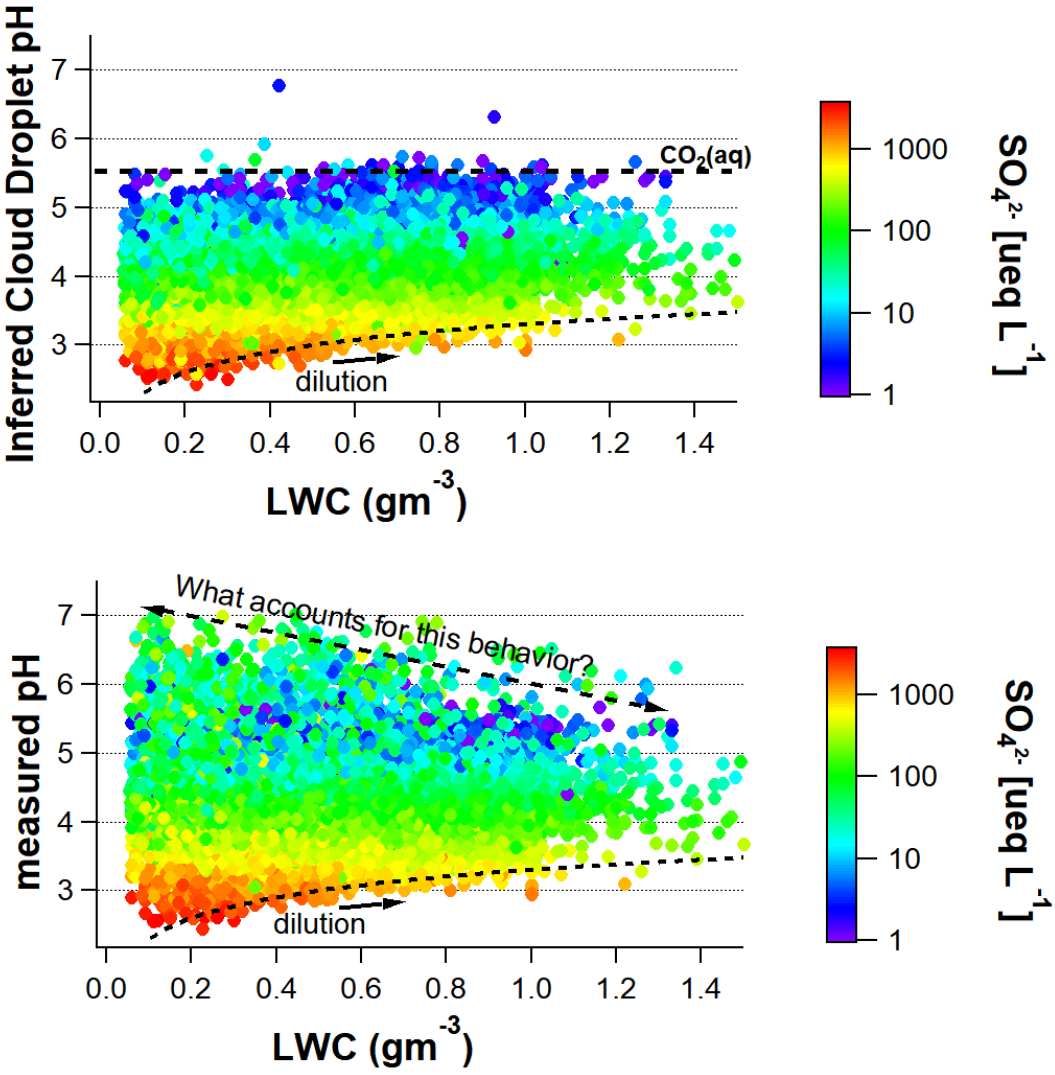

Figure S18. a) Measured bulk cloud water pH, and b) estimated cloud droplet pH as a function of the reported average Liquid Water Content (LWC) for all cloud water samples from 1994 to 2021, colored by measured sulfate concentrations.

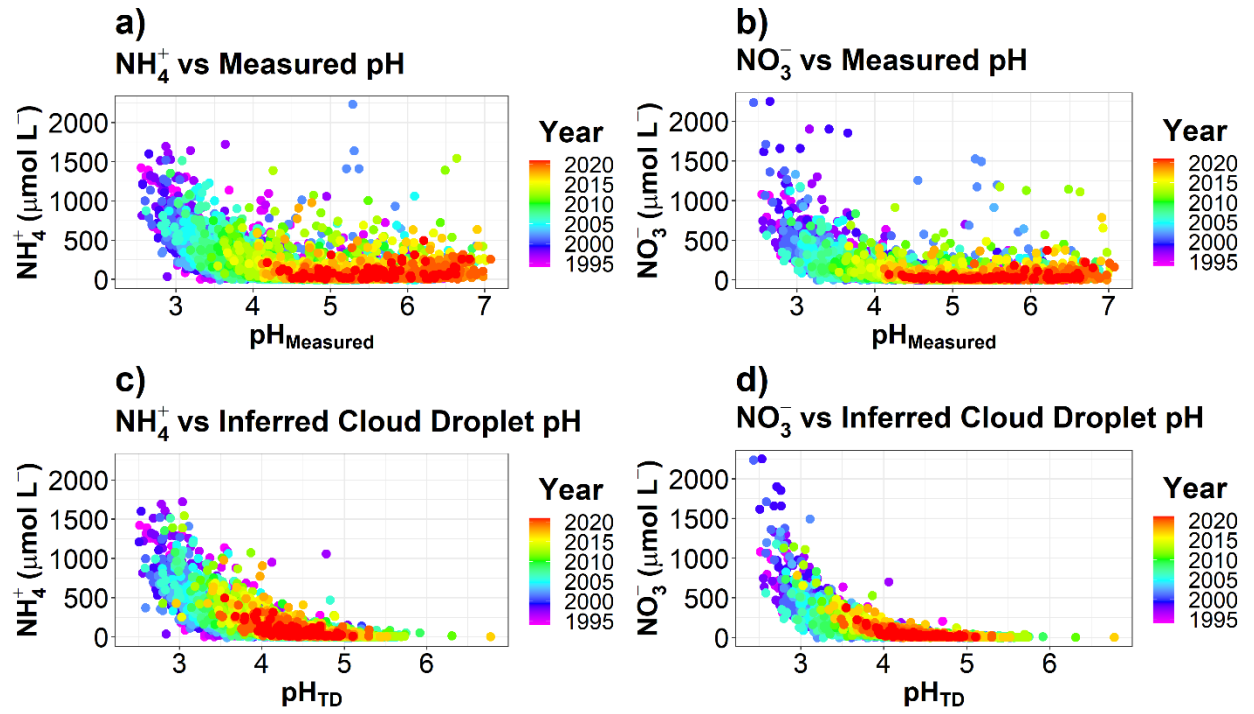

Figure S19. Measured NH_4^+ and NO_3^- concentrations versus a) and b) bulk cloud water pH, and c and d) pH_{TD}. Similar to TOC, the relationship between NH_4^+ and NO_3^- and pH is simplified when accounting for the influence coarse mode aerosol, with increasing concentrations of both analytes associated with lower pH_{TD}.

Section S16. Wildfire Smoke Influence at Whiteface Mountain

A WRF-Chem forecast shows elevated levels of CO attributed to wildfire smoke on July 15, 2021, with associated high levels of PM2.5. Five days later, the WRF-Chem forecast shows similar elevated levels of wildfire CO and PM2.5 over the Northeastern United States, further indicating an influence of Canadian wildfires impacting WFM (Fig. S20). More information about this WRF-Chem forecast can be found in Kumar et al. (2021). 5-day ensemble HYSPLIT back-trajectories launched on July 20, 2021 indicate the source location of the air mass originated from Eastern Manitoba, Canada, and Northeast North Dakota.

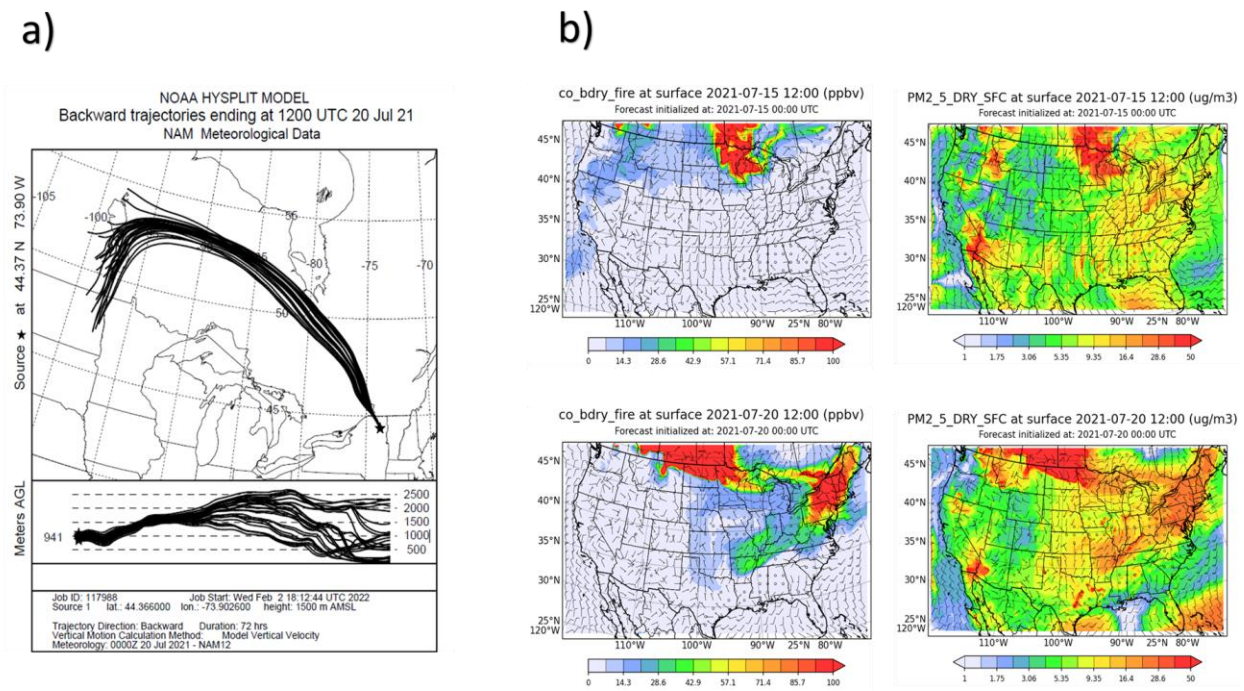

Figure S20. a) 5 day ensemble HYSPLIT back-trajectories using North American Mesoscale (NAM) 12 meteorological data launched on July 20th, 2021 at 12:00 UTC. b) WRF-Chem Forecast of carbon monoxide (CO) from boundary layer fires and surface PM 2.5 on July 15th, 2021 and on July 20th, 2021. A clear source of wildfire smoke emissions over Manitoba, Canada occurred on July 15th that eventually impacted air quality in New York on July 20th.

References

Aleksic, N. and Dukett, J. E., (2010). Probabilistic relationship between liquid water content and ion concentrations in cloud water, Atmospheric Research, 98, 400–405, https://doi.org/10.1016/j.atmosres.2010.08.003

Hansen, J. C., Woolwine III, W. R., Bates, B. L., Clark, J. M., Kuprov, R. Y., Mukherjee, P., Murray, J. A., Simmons, M. A., Waite, M. F., Eatough, N. L., Eatough, D. J., Long, R., and Grover, B. D., (2010). Semicontinuous PM2.5 and PM10 Mass and Composition Measurements in Lindon, Utah, during Winter 2007. Journal of the Air & Waste Management Association, 60, 346–355, https://doi.org/10.3155/1047-3289.60.3.346

Hrdina, A., Murphy, J. G., Hallar, A. G., Lin, J. C., Moravek, A., Bares, R., Petersen, R. C., Franchin, A., Middlebrook, A. M., Goldberger, L., Lee, B. H., Baasandorj, M., and Brown, S. S., (2021). The role of coarse aerosol particles as a sink of HNO_3 in wintertime pollution events in the Salt Lake Valley, Atmospheric Chemistry and Physics, 21, 8111–8126, https://doi.org/10.5194/acp-21-8111-2021

Kaewthong, P., & Wattanachant, S. (2018). Optimizing the electrical conductivity of marinade solution for water-holding capacity of broiler breast meat. Poultry science, 97(2), 701-708, https://doi.org/10.3382/ps/pex334

Kumar, R., Bhardwaj, P., Pfister, G., Drews, C., Honomichl, S., and D'Attilo, G. (2021). Description and Evaluation of the Fine Particulate Matter Forecasts in the NCAR Regional Air Quality Forecasting System, Atmosphere, 12, 302, https://doi.org/10.3390/atmos12030302

VandenBoer, T. C., Petroff, A., Markovic, M. Z., and Murphy, J. G., (2011). Size distribution of alkyl amines in continental particulate matter and their online detection in the gas and particle phase, Atmos. Chem. Phys., https://doi.org/10.5194/acp-11-4319-2011